Phys. Biol. **9** (2012) 066006 (9pp) doi:10.1088/1478-3975/9/6/066006

Branching geometry induced by lung self-regulated growth

Raphaël Clément[1,2], **Stéphane Douady**[2,3] **and Benjamin Mauroy**[1,3]

[1] Laboratoire J-A Dieudonné, UMR CNRS 7531, Parc Valrose, Université Nice Sophia Antipolis, F-06100 Nice, France
[2] Laboratoire Matière et Systèmes Complexes, UMR CNRS 7057, Université Paris Diderot, 10 rue A. Domon et L. Duquet, F-75013 Paris, France

E-mail: clementr@unice.fr

Received 31 May 2012
Accepted for publication 18 September 2012
Published 16 November 2012
Online at stacks.iop.org/PhysBio/9/066006

Abstract
Branching morphogenesis is a widely spread phenomenon in nature. In organogenesis, it results from the inhomogeneous growth of the epithelial sheet, leading to its repeated branching into surrounding mesoderm. Lung morphogenesis is an emblematic example of tree-like organogenesis common to most mammals. The core signalling network is well identified, notably the *Fgf10*/*Shh* couple, required to initiate and maintain branching. In a previous study, we showed that the restriction by SHH of *Fgf10* expression domain to distal mesenchyme spontaneously induces differential epithelial proliferation leading to branching. A simple Laplacian model qualitatively reproduced FGF10 dynamics in the mesenchyme and the spontaneous self-avoiding branching morphogenesis. However, early lung geometry has several striking features that remain to be addressed. In this paper, we investigate, through simulations and data analysis, if the FGF10-diffusion scenario accounts for the following aspects of lung morphology: size dispersion, asymmetry of branching events, and distal epithelium–mesothelium equilibrium. We report that they emerge spontaneously in the model, and that most of the underlying mechanisms can be understood as dynamical interactions between gradients and shape. This suggests that specific regulation may not be required for the emergence of these striking geometrical features.

S Online supplementary data available from stacks.iop.org/PhysBio/9/066006/mmedia

Introduction

Mammalian tree-like airways develop during the embryonic period, and early morphogenesis consists of the repeated branching of bronchial epithelium into lung mesenchyme. The molecular actors at work throughout this period are now relatively well known, and several pathways involved in growth regulation have been identified during the past two decades [1, 2]. However, the actual mechanisms of shape emergence remain unclear, especially if we consider certain aspects of lung branching geometry. Lung airways have indeed several non-trivial features that have, to our knowledge, not or little been addressed before. First, the tree is self-avoiding: bronchi never meet one another during morphogenesis. Second, distal epithelial buds, while being a site of important proliferation, never reach the mesothelium enclosing lung's mesenchyme. This suggests that bud tips somehow reach a dynamical equilibrium with the facing mesothelium. Third, the tree is far from being as regular as it is often described to be [3]: not only branches diameters and lengths are prone to significant variations within the same generation and from one individual to the other, but it is very well documented that branching events are mainly asymmetric, and this asymmetry has been reported to play an important role in lung efficiency [4, 5]. Finally, morphometric data suggest that successive generations of bronchi are smaller and smaller, with an average homothety ratio of about 80%.

[3] These authors contributed equally to work.

Most of the attempts made to describe or to model lung development, qualitatively or quantitatively, do not address the emergence of these striking features of the shape [6–11]. However, any attempt to model morphogenesis should be able to account for such characteristics, as they must somehow witness the mechanisms involved in shaping. In a previous paper, we proposed a new scenario for lung branching morphogenesis, together with qualitative modelling, numerical simulations and experiments [12]. The model integrates the core signalling network involved, and the geometry and diffusion relevant to lung early development. In particular, the elementary branching mechanism and the organization mechanism were discussed. We showed that the expression pattern of the *Fibroblast growth factor 10* (*Fgf10*), spatially restricted by *Sonic HedgeHog* (SHH) [13, 14], implies the diffusion of the proteic product FGF10 from distal mesenchyme towards epithelium. We found that diffusion in this geometry leads to a growth instability of the bronchial epithelium, which undergoes spontaneous branching instead of merely inflating as one could expect. We reported that this very mechanism also accounts for the self-avoiding feature of the tree.

In this paper, we detail further analysis of the fundamental branching mechanism uncovered thanks to the Laplacian model. We are willing to investigate the emergence of the previously enumerated features of the bronchial tree, through qualitative and/or quantitative comparison of the model-grown trees to available lung data. Both the questions and findings are original and of major importance in the understanding of morphogenesis mechanisms. Indeed, most of the growth models found in literature, whether they are confronted to data or not [11, 9], are algorithmic models with specific instructions: new branch creation, rotation, etc. Consequently, they do not allow the identification of branch formation mechanisms. Here we provide evidence that the mere diffusion of FGF10 from distal mesenchyme in fact accounts for the following features of the shape: dispersion in size, distribution of asymmetry ratios, and convergence towards an epithelium–mesothelium equilibrium. For comparisons, we used the human morphometric data collected and made available by Raabe *et al* in 1976 [15], as it includes for each branch its length, diameter, generation and related mother and daughters branches. The question of the confrontation of a model at early stages of morphogenesis to mature lung data is addressed later in the paper. Finally, the problem of the homothety ratio between generations is not specifically examined in this work, although a qualitative scenario is discussed.

Results

The lung morphogenesis model

In this section, we will quickly present the morphogenesis model used in the rest of the paper. It was first introduced and widely discussed in a previous article [12]. During early lung morphogenesis, the central proliferation role of FGF10 has been identified since the 1990s [14, 16, 17]. In particular, null mutants of *Fgf10* or its receptor *Fgfr2b* have been reported to present lung agenesis [18, 19]. *Fgf10* expression is spatially restricted to the distal mesenchyme by SHH. FGF10 thus diffuses from distal mesenchyme towards epithelium, where it induces epithelial proliferation. The diffusion process is physically driven by the gradient of FGF10 concentration, with a maximum concentration near the expression site (distal mesenchyme) and a minimum concentration near the reception sites (epithelium). We proposed and confirmed that the concentration c of the FGF10 protein within the mesenchyme is well described by Laplace's diffusion equation:

$$\nabla^2 c = 0. \tag{1}$$

The steady state assumption supposes that growth is slower than diffusion. This is consistent with the widely reported observation of *Fgf10* expression domain spatial stability during growth: it remains restricted to the distal mesenchyme. The boundary conditions are related to *Fgf10* expression and FGF10 binding to FGFR2b. They consist in a maximal concentration $c_{\max}$ on the distal boundary where *Fgf10* expression is strong (mesothelium), and in a minimal concentration $c_{\min}$ on the epithelial sheet where the protein is received and degraded. Growth is simply computed as a function of FGF10 flux received. As diffusion tends to spatially equilibrate concentration, the local diffusive flux is proportional to the local gradient of concentration. The motion of both boundaries is thus written as follows:

$$\begin{cases} u_e = f(\nabla c) \\ u_m = (1+g) f(\nabla c). \end{cases} \tag{2}$$

u_e and u_m respectively stand for the normal velocity of the epithelial and mesothelial sheets. The growth response f is theoretically underlain by lung regulatory network and by the mechanical properties of the epithelium–mesenchyme interface. Practically, we use smooth threshold functions (sigmoid), with threshold G_0 and threshold width σ. Growth dependence to gradient rather than concentration has been deeply discussed in our previous paper. While it is often assumed that cells are sensitive to concentration, sensitivity requires measuring an amount of interactions per unit of time. Unless it moves quickly in the medium, a receptor cannot count surrounding particles, but needs to count how many particles reached it through diffusion. Here FGF10 binds to FGFR2b only if the first 'hits' the second, and the amount of FGF10 received by epithelial cells is consequently related to the flux (thus to the gradient). This hypothesis was well confirmed by our previous work [12], in particular we showed that it explains the patterning of FGF10-induced genes such as *Spry2*. The experimental fact that homogeneous addition of exogenous FGF10 does not cause branching failure [20] may be opposed to a flux-based sensitivity. This is in fact not a valid argument, since in these experiments, FGF10 consumption by epithelial cells will quickly restore a gradient. The parameter g stands for mesenchymal proliferation, and the corresponding term $gf(\nabla c)$ in u_m is discussed in our first paper. Simulations based on this model showed that the initial epithelial tube robustly undergoes repeated branching, that the tree formed is self-avoiding and that the distal buds never reach the mesothelium. This is spontaneous as no branching routine of any kind is implemented in the model.

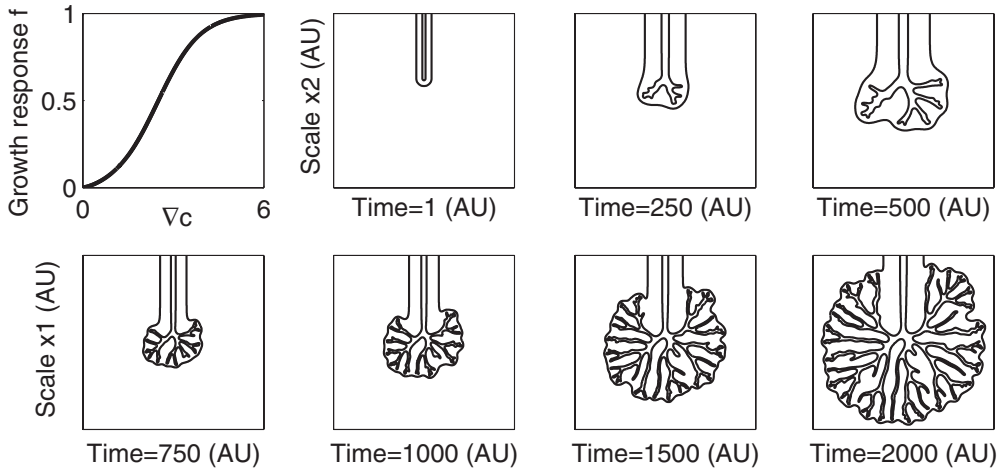

Figure 1. Typical numerical simulation with the corresponding growth response f ($\lambda = 0.075$, $g = 5$). Subfigures are time-lapse images of the simulation, from initial condition (time step 1) to simulation stop (time step 2000). There is a factor two in magnification between the first and the second line. All values are given in arbitrary units (AU).

Branching relies on the instability of the epithelial sheet: spatial perturbations are amplified as they locally increase the concentration gradient, and thus the received flux of FGF10. When the space between two growing branches decreases, the local gradient is locally reduced, which prevents from branches collision. A typical run is presented figure 1. In the simulations, equations are solved thanks to the finite elements method. We called λ the interfacial resolution of the mesh used to solve Laplace equation. As discussed later in the paper, λ has an implicit physical role. Please refer to supplementary data for more details concerning the simulations (available at stacks.iop.org/PB/9/066006/mmedia).

Branches typical sizes and dispersion in size

Lung is often mistakenly considered as a regularly branching dichotomous tree. While the first generations have been reported to be very stereotyped, it seems that later generations rather fill available space than follow a stereotyped routine [21]. Weibel reported that there is important dispersion in branches sizes, even among a unique generation [3], and that branching events are irregularly spaced. While it is very useful to consider an averaged tree for shape analysis purposes or to model flow in the tree [22], dispersion in sizes is inherent to morphogenesis mechanisms, and understanding these mechanisms therefore requires accounting for this dispersion. In this section we analyse the typical sizes and size dispersion. For each branch, the length is noted l and the diameter w. Morphometry measurements of adult lungs are taken from Raabe *et al* data. Information and references concerning data collection are provided in the supplementary data (available at stacks.iop.org/PB/9/066006/mmedia). Measurements from growth simulations are numerically implemented: a hierarchic skeleton of the tree is computed thanks to the Voronoi diagram, and allows extracting relevant distances (AU). A more precise description of the computational techniques is available in the supplementary data (supplementary figure 1 (available at stacks.iop.org/PB/9/066006/mmedia)). It could seem questionable to compare mature lungs geometry to the

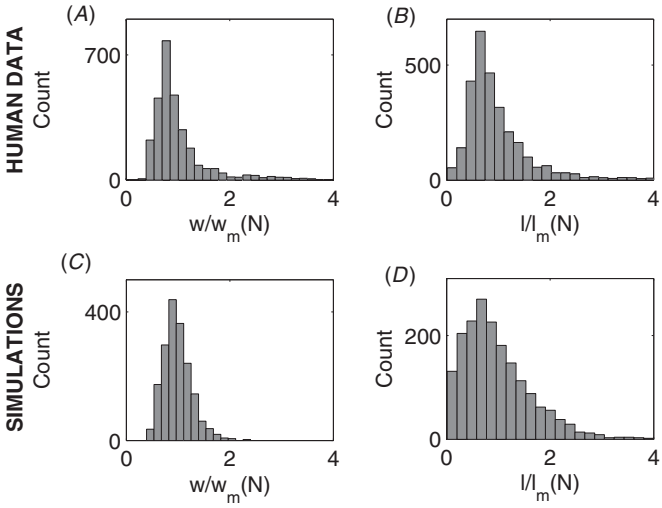

Figure 2. (*A*),(*B*) Human data. (*C*),(*D*) Simulations ($\lambda = 0.075$, $g = 5.5$). (*A*),(*C*) Distribution of branches diameters rescaled by the mean diameter of the corresponding generation. (*B*),(*D*) Distribution of branches lengths rescaled by the mean length of the corresponding generation.

results of an early morphogenesis model. The assumption is that features of the shape, such as asymmetry or size dispersion, are not a consequence of aging but rather inherent to morphogenesis. Although this is a little discussed matter in relevant literature, available data shows that this is indeed the case: variability in branches size and asymmetry are present at developmental stages.

Analysis of Raabe data shows that typical length scales exist in the bronchial tree. Figure 2(*A*) shows the distribution for diameters. Values are rescaled with respect to the mean diameter $w_m(N)$ of the corresponding generation N, which allows to represent all generations on one histogram. Similarly, figure 2(*B*) shows the histogram for branches lengths rescaled by the mean length of the corresponding generation, $l_m(N)$. We clearly obtain a peak near the mean rescaled value, for both diameter and length. However, there is in both cases a

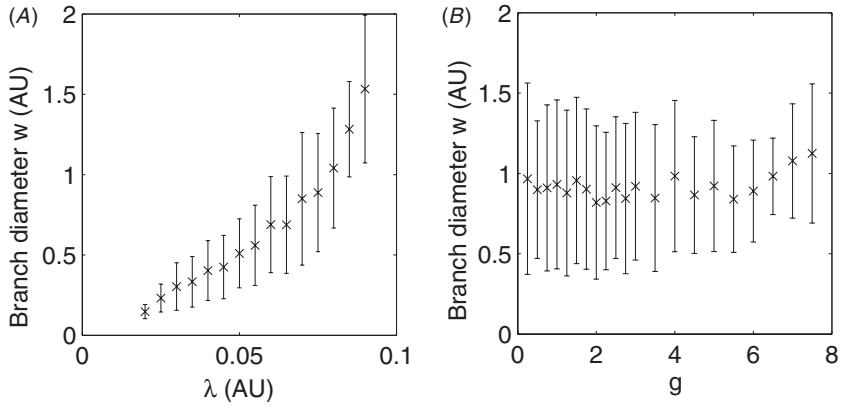

Figure 3. (*A*) Mean diameter of formed branches as a function of the cut-off length λ (with $g = 5$). (*B*) Mean diameter of formed branches as a function of the mesenchymal proliferation term g (with $\lambda = 0.075$). Error bars represent the standard deviation.

significant dispersion around the mean rescaled value. Also, the distributions are not normal, as the peaks are right-tailed.

These observations are not trivial, and we wanted to test the model to find out if the dispersion in size was similar. We computed similar measurements on model-generated trees. To keep the comparison to data relevant, we used the same rescaling techniques and plotted the rescaled diameters and lengths distributions (figures 2(*D*), (*E*)). We found a good agreement between human data and model-generated trees: distributions shapes obtained are very similar: they are not normal and present a right tail. However, quantitative discrepancies can be noted, such as the tail's thickness or the width of the distributions. Since the model is built on the growth response to FGF10, it is very likely that a more realistic growth response would be required to achieve a better accuracy. While this would prove very interesting for future studies, the purpose of this model is not quantitative fitting but rather the identification of mechanisms. We have here evidence that FGF10 diffusion alone provides a qualitative explanation for size dispersion: as branch formation is spontaneous in the model, the fact that the model qualitatively reproduces the size distribution is not trivial. It also suggests that size dispersion may not require specific regulation, but may rather be a consequence of the growth instability underlain by FGF10 diffusion from distal mesenchyme. Although in both cases (data and simulations) we considered branches altogether, it is worth noting that the global shape of the distributions does not change with the generation.

In our previous paper, we discussed the possible origins of the typical size, in particular the rigidity of the epithelium–mesenchyme interface. Here we confirm that the 'persistence length' of the epithelial sheet plays a central role. In the model, this mechanical persistence length is implicit, and computed as the spatial resolution of the epithelium–mesenchyme interface λ [12]. It is equivalent to a persistence length since nothing can be observed under this length scale: possible perturbations of the surface are smoothed. Physically, it denotes the stiffness of the epithelial sheet, in other words the strength of cell–cell bonds. In some way, it is similar to the capillary length known to play a central role for size selection in the viscous fingering instability [23]. We plotted the mean diameters of the model-generated trees against the cut-off length λ. Similarly to what was found in viscous fingering for the capillary length, the mean value of branches diameter increases with λ (figure 3(*A*)).

Although this suggests that epithelial stiffness may play a role in branches diameters, this is not a definitive answer to the question of size selection: additional experiments are required to confirm this hypothesis. Also, other parameters are known to have an influence on branches sizes: Unbekandt *et al* for instance reported that trachea occlusion, by increasing lumen's pressure, had an influence on the growth rate and on branches size [24]. It is worth noting that the value of g, that stands for mesenchymal proliferation, has no influence on branches size (figure 3(*B*)), although it has a strong influence on the epithelium–mesothelium distance, as discussed later in the paper.

Asymmetry of branching events

Morphometric studies have, among others, focused on the asymmetry of branching events. In this work we define the asymmetry ratio of a branching event as the ratio between the diameters of the two daughter branches, i.e. $A = w_1/w_2$ with $w_1 \leqslant w_2$. The closest A is to 1, the more symmetric is the branching event. The average value of A is roughly 0.8 in humans. Although small variations exist among individuals and in other species, the mean ratio is very robust and remains close to this value. The asymmetry ratio has also been reported to play an important role in adult lung efficiency [4, 5]. Data made available by Raabe *et al* allows extracting the ratios, as branches size are provided together with their hierarchic position in the tree. It is then easy, for a given branch, to measure the asymmetry ratio of the associated daughter branches. Figure 4(*A*) displays the distribution of asymmetry ratios obtained from human data (generations 1 to 11). There is important dispersion in asymmetry ratios, with a mean value of 0.80. It is worth noting that the last column (A close to 1) is surprisingly high. There is in fact a bias related to data collection, as measurements are rounded to the closest 0.1 mm. For small branches with a typical diameter of a few tenths of mm (a lot of branches, since the number of branches increases with the generation), this represents an important error and implies an accordingly important chance to measure a ratio of exactly 1. The last column thus includes many branching

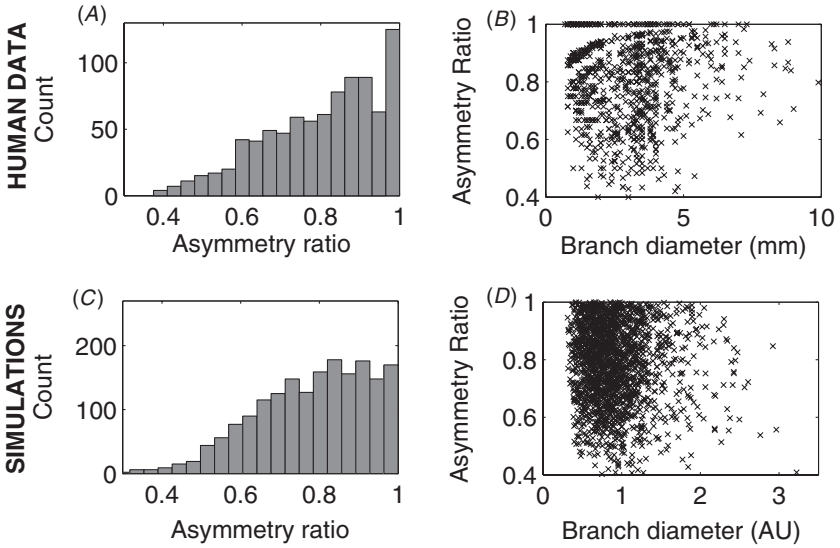

Figure 4. (*A*), (*B*) Human Data. (*C*), (*D*) Simulations ($\lambda = 0.075$, $g = 5.5$). (*A*), (*C*) Distribution of the asymmetry ratios. (*C*), (*F*) Asymmetry ratio versus diameter of the mother branch for all branching events. No apparent correlation is found.

events with measured ratio exactly equal to 1, that should in fact stand in neighbouring columns. Searching for the possible influence of branches size on the asymmetry ratio, we also compared the diameter of the mother branch to the asymmetry of the related branching event. Figure 4(*B*) shows that the diameter of the mother branch has no noticeable influence on the asymmetry ratio.

Again, we wanted to investigate if the instability mechanism underlain by FGF10 diffusion and described by our Laplacian model accounted for asymmetric branching events. We computed the hierarchic skeleton of the final shapes. Information for each branch includes sizes and position in the tree, and similarly allows extracting asymmetry ratios. Figure 4(*C*) displays the distribution of asymmetry ratios obtained from model-generated trees. Similarly to what we observed in available lung data, we found that the average branching event is asymmetric, and that the mean asymmetry ratio equals 0.78 for the set of parameters used, compared to 0.80 in Raabe data. The distribution is qualitatively very similar, except for the peak of $A = 1$, which, as discussed, is biased. Figure 4(*D*) shows that the asymmetry ratio of a branching event is not correlated to the size of the mother branch, as it was found for Raabe data. Again, the data and model distributions are non-trivial and very similar, suggesting that specific regulation may not be required to achieve the statistical asymmetry of the branching events.

Further analysis of the model-generated trees suggests that the value of the asymmetry ratio is very robust. It is worth noting that no fitting or parameters adjustment was done to achieve a ratio of 0.78. However small but coherent variations of A were observed when available parameters were modified. We hypothesized that these variations may be related to the ratio of occupied space: as it modifies the growth rate distribution along the tip, it modifies the probability distribution to develop an instability. Therefore we designed specific simulations to address this question: a unique epithelial tube is grown in an epithelial sector of fixed angular opening. This mimics the presence of neighbouring branches at a certain distance. Growth is implemented thanks to the same model until a branching event occurs and two daughters branches are formed. For each angular opening dozens of independent runs are made, and a mean asymmetry ratio is obtained. As shows figure 5, the mean asymmetry ratio has only small absolute variations, but is clearly higher when the angular opening is small. When the angle is increased, the asymmetry ratio tends towards a limit value standing between 0.6 and 0.7. This suggests that the close and restrictive presence of neighbouring branches stabilizes branching events and involves more symmetric trees, whereas branching events are more asymmetric when available space is important.

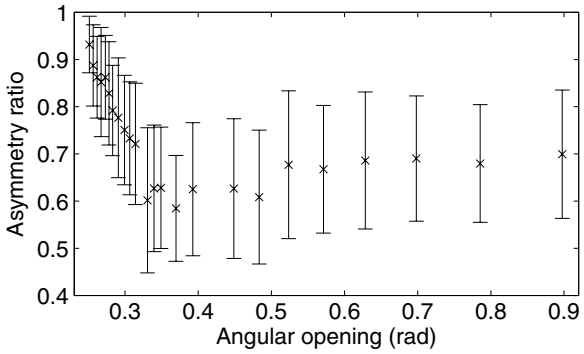

Figure 5. Mean asymmetry ratio (averaged from 60 to 100 runs) versus angular opening in simulations where a unique epithelial tube is grown in an angular sector ($\lambda = 0.075$, $g = 3$). Error bars represent the standard deviation.

The influence of space-filling on A should be interpreted as a geometrical effect of the diffusion process. As FGF10 concentration on the whole epithelium is $c_{\min}$, the neighbouring presence of branches lowers the gradient of FGF10 on the sides of the branch. The closer are the neighbouring branches, the more FGF10 flux is focused on bud's tip. The growth rate distribution along the tip is thus narrower. As spatial perturbations are more susceptible to

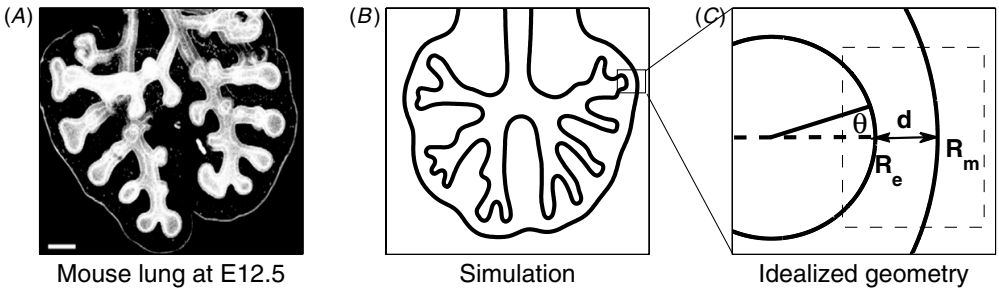

Figure 6. (*A*) Mouse lung at E12.5 stained for E-Cadherin (courtesy of E Keshet [25], adapted with permission from *Development*). One can clearly identify a well-defined distance between distal tips and mesothelium. Scale bar is 200 μm. (*B*) Simulation at time step 300 ($\lambda = 0.075$, $g = 3$). A similar well-defined distance between tips and mesothelium is observed. (*C*) Idealized circular geometry for the calculation. We consider a unique epithelial tip (radius of curvature R_e) at a distance d from mesothelium (radius of curvature R_m). The angle θ is the angle to the tip. The dashed rectangle schematically delimits the area of interest.

develop and induce branching if they have an important growth rate, i.e. if they are closer to the tip, branching events are statistically more symmetric. When neighbouring branches are far, on the contrary, the growth rate distribution spreads on the tip. The results suggest that beyond a certain angle, this geometrical effect is too weak to induce an effective change in gradient distribution. In other words, branches do not 'sense' each other beyond a certain distance (here, angle). It is worth noting that in model-generated trees, we were unable to achieve mean ratios under 0.7, suggesting that spontaneously forming trees are always in a 'self-sentient' regime (left part of the curve).

As space-filling is of major importance for lung function and efficiency, one could hypothesize that lung morphogenesis stands in a highly-filled volume regime. This is partly confirmed by figure 7: an asymmetry ratio of 0.8 corresponds to small angular openings, and to a regime in which branches do sense their neighbours. This could also explain the small variations in asymmetry ratio observed from one individual to the other, or from one species to the other: in this regime, small variations in available space do affect the mean asymmetry ratio. Direct measurements of the space actually occupied in several individuals would be useful to confirm this last hypothesis.

Epithelium–mesothelium equilibrium

Observation of lung development reveals another striking feature of the shape. Epithelial buds, although they are major sites of proliferation, never reach the mesothelium enclosing the mesenchyme (figure 6(*A*)). Looking more closely at this aspect of the shape, available imaging reveals that all buds stand at a comparable distance of the mesothelium during growth: the sac enclosing the growing organ develops in such way that a dynamical equilibrium is reached between distal epithelium and mesothelium. Although this is again not trivial, the question has to our knowledge never been addressed in relevant literature. No information related to this distance can be extracted from the data collected by Raabe *et al*, but qualitative observations at various stages of development and in various species suggest that the existence of such an epithelium–mesothelium equilibrium is a general feature of lung development. Bronchi would otherwise penetrate the pleural mesothelium. In the model, this equilibrium appears spontaneously, as shown by simulations (figure 6(*B*)); again this suggests that no specific regulation is required to achieve the equilibrium, as it seems inherent to the mechanism underlain by FGF10 diffusion from distal mesenchyme. In this section we will discuss the mechanisms involving this equilibrium.

Measurements of the distance d from distal tips to mesothelium after a simulation has ended allows testing the influence of the available parameters on the distance, and reveals that d mainly depends on the value of g (figure 7(*A*)). This is rather intuitive: the distance between epithelium and mesothelium depends on relative mesenchymal proliferation. It is worth noting that the cut-off length λ, that had critical influence on branches size (figure 3(*A*)), seems to have no influence on the distance (figure 7(*B*)). Similarly, g had no influence on the branches size (figure 3(*B*)). This suggests that d may be another typical length scale emerging during lung development.

Measurements of the evolution of d suggests that it does not converge as the tree grows: it slowly increases with the size of the tree. Thus we rescaled this distance by the radius of curvature R_m of the closest point of the mesothelium: $\tilde{d} = d/R_m$. This rescaled distance converges in simulations towards an equilibrium value $\tilde{d}_{\text{eq}}$. To understand the dynamics of a bronchial tip, we focused on the local geometry of the bud and its surroundings. Let us consider a portion of epithelium (distal tip) with radius of curvature R_e, separated by a distance d from a portion of mesothelium with radius of curvature R_m. We are interested in the dynamics of these local observables, and in particular in the dynamics of the rescaled distance, $\tilde{d}$. We do not consider the rest of the tree, and approximate this local geometry with two circles of radii R_e and R_m (figure 6(*C*)). In the general case, the circles are not concentric. The exact expression of the Laplacian concentration can be calculated thanks to a conformal mapping of the concentric solution, which then leads to the exact expressions of the gradient $(\nabla c)_{\text{epi}}$ and $(\nabla c)_{\text{meso}}$ along epithelium and mesothelium respectively. As we focus on the tip's behaviour, we only consider small angles, and can develop the expressions of the

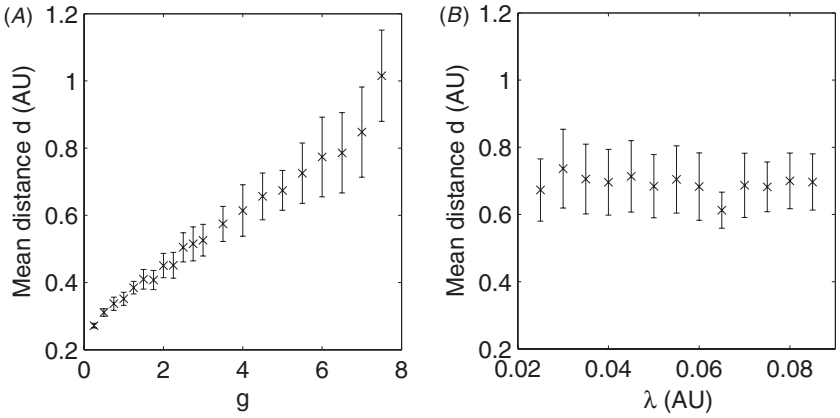

Figure 7. (*A*) Mean distance from distal tips to mesothelium as a function of the mesenchymal proliferation term g (with $\lambda = 0.075$). (*B*) Mean distance from distal tips to mesothelium as a function of the cut-off length λ (with $g = 5$). Error bars represent the standard deviation.

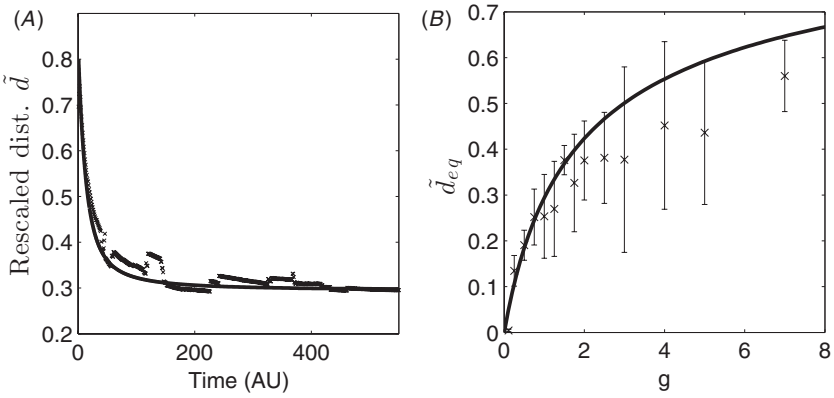

Figure 8. (*A*) Time evolution of the rescaled distance to mesothelium $\tilde{d}$ of an epithelial tip during a typical linear simulation ($g = 1$, dotted line); and corresponding prediction of the local calculation (solid line), starting from identic initial conditions. In both cases, $\tilde{d}$ tends towards an equilibrium value $\tilde{d}_{\text{eq}}$. (*B*) Mean value of $\tilde{d}_{\text{eq}}$ as a function of the mesenchyme proliferation term g; and $\tilde{d}_{\text{eq}}(g)$ predicted by the calculation (solid line). Error bars represent the standard deviation.

gradient at the second order in the angle θ (with $\theta = 0$ at the tip, see figure 6(*C*)):

$$\begin{cases} (\nabla c)_{\text{epi}} = a_e + b_e\theta^2 \\ (\nabla c)_{\text{meso}} = a_m + b_m\theta^2. \end{cases} \tag{3}$$

Coefficients a_e, b_e, a_m and b_m are functions of R_e, R_m, and d. Details of the calculation are provided in the supplementary data (available at stacks.iop.org/PB/9/066006/mmedia). Like in the simulations, growth is a function of the gradient, and thus here of the angle θ. This involves an evolution of the curvatures and of the distance. We are then able to write the evolution of the three variables d, R_e and R_m. With the dot denoting the temporal derivative, it reads:

$$\begin{cases} \dot{R}_e = f(a_e) - 2b_e f'(a_e) \\ \dot{R}_m = (1+g)[f(a_m) - 2b_m f'(a_m)] \\ \dot{d} = (1+g)f(a_m) - f(a_e). \end{cases} \tag{4}$$

Given initial conditions for R_e, R_m and d, we can solve this system numerically. Starting with the initial condition used in growth simulations, we can directly compare the evolution of $\tilde{d}$ in the simulations to the evolution of $\tilde{d}$ predicted by equation (4). We focus here on linear growth responses for simplicity purposes and will discuss the importance of f shape. A direct comparison is provided for a typical simulation on figure 8(*A*). There is good agreement between the numerical experiment and the prediction, and $\tilde{d}$ converges toward an equilibrium value $\tilde{d}_{\text{eq}}$. Solving the system (equation (4)) until the equilibrium is reached with various values of g, we can predict a theoretical dependence of $\tilde{d}_{\text{eq}}$ relatively to g, and compare the curve obtained to the curve built with measurements from numerical simulations (figure 8(*B*)). The agreement is very good for small values of g. For higher values of g, the predictive curve overestimates the value of $\tilde{d}_{\text{eq}}$. This was to be expected, since in the two circles model the influence of neighbouring branches was neglected, which is abusive for large values of g. When the distance to mesothelium is small (small g), the gradient at the tip is mostly determined by the close presence of the mesothelium: the two circles approximation is good. When the distance is important (high g), the presence of neighbouring branches modifies the gradient distribution, and the circles approximation becomes bad.

The main idea behind these results is that the interplay between the two moving boundaries, the epithelium and the mesothelium, involves spontaneous regulation of tips growth. This dynamics is original and, to our knowledge, is reported here for the first time, although it is likely to exist in other

organs or physical systems. The results presented here show that this self-regulation exists in the lung thanks to the spontaneous dynamics of bud tips shape and curvature. Indeed, it implies that FGF10 concentration gradient, very sensitive to local geometry, is such that $\tilde{d}$ is kept constant. In other words, the distance d and curvature radii R_e and R_m at bud tip are determined by the ratio between u_e and u_m. From a theoretical point of view, this is how g controls $\tilde{d}_{\mathrm{eq}}$. This is in fact very intuitive: proliferation between epithelium and mesothelium partly controls the distance and the curvatures. It is also intuitive that $\tilde{d}_{\mathrm{eq}}$ tends to 0 when g tends to 0: mesenchymal proliferation is actually required to prevent any epithelium–mesothelium contact, as observed during lung development. Extensive study with various growth responses will be useful to confirm that behaviour. However, sigmoid-based simulations presented in this paper suggest that this is indeed the case, although no quantitative comparison between simulations and calculation is provided. Also, additional in vivo measurements and fine imaging of bud tips shapes and aspect ratios would prove very interesting in the light of these findings.

Discussion

Specific regulation may not be required

In this paper, we analysed various aspects of lung morphogenesis thanks to a simple model based on FGF10 diffusion from distal mesenchyme, first introduced in a previous article. We want to point out that the purpose of such a model is not to actually fit lung development or to quantitatively predict lung morphology; but rather to identify the mechanisms involved in pattern formation and in the emergence of the striking features of the shape. The strong qualitative agreement obtained between the model and the observation suggests that no specific regulation is required to achieve these features. However, it is likely that they are regulated by other pathways. This is consistent with available mutant data: except from null mutants of *Fgf10* or *Fgfr2b*, displaying agenesis, and null mutants of *Shh*, displaying branching failure, mutations only lead to 'minor' shape changes, with no loss of these features. The fact that *Shh* null mutants lungs fail to branch is also consistent with the model, as the restriction of *Fgf10* expression to distal mesenchyme is lost.

Homothety ratio between generations

An important aspect of lung development which has not been specifically addressed in this paper is the homothety ratio between generations. However, the following hypothesis can be made. In the model, proliferation (and thus, growth) is only triggered by FGF10 flux. But in addition to this differential FGF10-induced growth, there may be homothetic growth, unrelated to FGF10. Even if the typical size of newly formed branches does not change throughout generations, older branches would continue to grow homogeneously. This scenario naturally leads to a final tree with branches with decreasing sized along the generations. Simulations, not provided here, confirm this hypothesis. To confirm if this is the actual mechanism at work during lung development, measurements of branches diameters at the very moment they form will be required.

Side-branching and tip-splitting

In this paper we do not introduce specific analysis for side-branching versus tip-splitting (and therefore stuck to the most common lung tree nomenclature, from proximal to distal branches). It is unsure that side-branching plays a significant role in lung development, as suggested by recent 3D reconstructions [21]: it is indeed hard to state whether there is side-branching or if this is irregular and/or asymmetric tip-splitting. Moreover, side-branching in Laplacian system is known to result from tip stabilization by external factors such as anisotropy or narrowing environment [26, 27], factors that are absent in our simplified 2D model, although they may exist in lung morphogenesis. Therefore, we do not think that the merging of all branching events into one category (which also happens to allow easy confrontation to available data, where the same was done) introduces a flaw in the conclusions of the paper, that lie in more general mechanisms of shape emergence.

Lung grows in three dimensions

A surprising fact is that a two-dimensional model allows such good agreement with three-dimensional lung data. In fact, the Laplacian instability mechanism modelled in 2D is perfectly relevant to 3D problems. This is well confirmed by our preliminary results of 3D simulations (figure 2 in supplementary data (available at stacks.iop.org/PB/9/066006/mmedia)). Despite very promising results, the important computation times involved by 3D simulations still prevent one from carrying out this study rigorously in 3D. But in the few runs performed, we similarly found that symmetry is broken, tip growth is favoured, typical length scales emerge with respect to the parameters used, and branches sizes spread around a typical length scale. The global mechanism thus seems conserved. More surprising is the conserved value of the asymmetry ratio. A possible explanation is the following: even in 3D, at the onset of a bifurcation, a branching plan is determined. This is a geometrical effect of the instability: the axisymmetry of the bud is broken and a branching plan is selected. Bud's growth rate distribution in this branching plan should be qualitatively similar to the 2D growth rate distribution, and should lead to very similar values of the asymmetry ratio. This argument is also relevant to the distribution of branches sizes, which should also rely on the growth rate distribution along bud tip. Calculations of the 3D growth rate in a plan could prove interesting to confirm this last hypothesis.

Conclusion

Finally, this work tends to confirm that FGF10 diffusion from distal mesenchyme not only accounts for branching morphogenesis, but also for many other features of the shape. The emergence of typical sizes (diameter and length) and the dispersion around the typical sizes are inherent to the growth instability, while asymmetry ratios and epithelium–mesothelium equilibrium result from dynamical and reciprocal

interactions between flux distribution (inducing growth and thus shape modification) and shape (that modifies gradients and thus fluxes). Altogether, these results suggest that the self-regulated instability mechanism, underlain by FGF10 diffusion from distal mesenchyme, may indeed be the master mechanism of early lung branching morphogenesis.

Acknowledgments

The authors thank Pierre Blanc and Vincent Sapin for early discussions; Etienne Couturier and Renaud Bastien for their helpful contributions concerning the computation of hierachic skeletons and the curvature measurements; and Yves Couder for fruitful discussions concerning tip-splitting and side-branching. Part of this work has been funded by the program 'Aide individuelle aux jeunes chercheurs' (City of Nice), and by the 'Plan Pluri Formation—Développement d'un pôle de Biologie Systémique' (University of Nice-Sophia Antipolis, 2008–2011).

References

[1] Warburton D, Bellusci S, de Langhe S, del Moral P-M, Fleury V, Mailleux A, Tefft D, Unbekandt M, Wang K and Shi W 2005 Molecular mechanisms of early lung specification and branching morphogenesis *Pediat. Res.* **57** 26R–37R

[2] Cardoso W V and Lü J 2006 Regulation of early lung morphogenesis: questions, facts and controversies *Development* **133** 1611–24

[3] Weibel E R 1963 *Morphometry of the Human Lung* (Berlin: Springer)

[4] Mauroy B and Bokov P 2010 The influence of variability on the optimal shape of an airway tree branching asymmetrically *Phys. Biol.* **7** 016007

[5] Florens M, Sapoval B and Filoche M 2011 Optimal branching asymmetry of hydrodynamic pulsatile trees *Phys. Rev. Lett.* **106** 178104

[6] Metzger R J and Krasnow M A 1999 Genetic control of branching morphogenesis *Science* **284** 1635–9

[7] Tebockhorst S, Lee D, Wexler A S and Oldham M J 2007 Interaction of epithelium with mesenchyme affects global features of lung architecture: a computer model of development *J. Appl. Physiol.* **102** 294–305

[8] Metzger R J, Klein O D, Martin G R and Krasnow M A 2008 The branching programme of mouse lung development *Nature* **453** 745–50

[9] Kitaoka H, Takaki R and Suki B 1999 A three-dimensional model of the human airway tree *J. Appl. Physiol.* **87** 2207–17

[10] Menshykau D, Kraemer C and Iber D 2012 Branch mode selection during early lung development *PLoS Comput. Biol.* **8** e1002377

[11] Tawhai M H, Hunter P, Tschirren J, Reinhardt J, McLennan G and Hoffman E A 2004 Ct-based geometry analysis and finite element models of the human and ovine bronchial tree *J. Appl. Physiol.* **97** 2310–21

[12] Clément R, Blanc P, Mauroy B, Sapin V and Douady S 2012 Shape self-regulation in early lung morphogenesis *PLoS ONE* **7** e36925

[13] Bellusci S, Furuta Y, Rush M G, Henderson R, Winnier G and Hogan B L M 1997 Involvement of sonic hedgehog (SHH) in mouse embryonic lung growth and morphogenesis *Development* **124** 53–63

[14] Bellusci S, Grindley J, Emoto H, Itoh N and Hogan B L M 1997 Fibroblast growth factor 10 (fgf10) and branching morphogenesis in the embryonic mouse lung *Development* **124** 4867–78

[15] Raabe O G, Yeh H C, Schum G M and Phalen R F 1976 *Tracheobronchial Geometry: Human, Dog, Rat, Hamster—A Compilation of Selected Data from the Project Respiratory Tract Deposition Models* (Albuquerque, NM: US Energy Research and Development Administration, Division of Biomedical and Environmental Research)

[16] Lebeche D, Malpel S and Cardoso W V 1999 Fibroblast growth factor interactions in the developing lung *Mech. Dev.* **86** 125–36

[17] Lü J, Izvolsky K I, Qian J and Cardoso W V 2005 Identification of fgf10 targets in the embryonic lung epithelium during bud morphogenesis *J. Biol. Chem.* **280** 4834–41

[18] Peters K, Werner S, Liao X, Wert S, Whitsett J and Williams L 1994 Targeted expression of a dominant negative fgf receptor blocks branching morphogenesis and epithelial differentiation of the mouse lung *EMBO J.* **13** 3296–301 PMCID: 395226

[19] Sekine K *et al* 1999 Fgf10 is essential for limb and lung formation *Nature Genet.* **21** 138–41

[20] Mailleux A A, Tefft D, Ndiaye D, Itoh N, Thiery J P, Warburton D and Bellusci S 2001 Evidence that sprouty2 functions as an inhibitor of mouse embryonic lung growth and morphogenesis *Mech. Dev.* **102** 81–94

[21] Blanc P, Coste K, Pouchin P, Azaïs J-M, Blanchon L, Gallot D and Sapin V 2012 A role for mesenchyme dynamics in mouse lung branching morphogenesis *PLoS ONE* **7** e41643

[22] Mauroy B, Filoche M, Weibel E R and Sapoval B 2004 An optimal bronchial tree may be dangerous *Nature* **427** 633–6

[23] Saffman P G and Taylor G I 1958 The penetration of a fluid into a porous medium or hele-shaw cell containing a more viscous liquid *Proc. R. Soc.* A **245** 312–29

[24] Unbekandt M, del Moral P-M, Sala F G, Bellusci S, Warburton D and Fleury V 2008 Tracheal occlusion increases the rate of epithelial branching of embryonic mouse lung via the fgf10-fgfr2b-sprouty2 pathway *Mech. Dev.* **125** 314–24

[25] Lazarus A, Del-Moral P M, Ilovich O, Mishani E, Warburton D and Keshet E 2011 A perfusion-independent role of blood vessels in determining branching stereotypy of lung airways *Development* **138** 2359–68

[26] Rabaud M, Couder Y and Gerard N 1988 Dynamics and stability of anomalous saffman-taylor fingers *Phys. Rev.* A **37** 935–947

[27] Lajeunesse E and Couder Y 2000 On the tip-splitting instability of viscous fingers *J. Fluid Mech.* **419** 125–49

Branching geometry induced by lung self-regulated growth

Supplementary Information

Raphaël Clément, Stéphane Douady, Benjamin Mauroy

July 24, 2012

Growth simulations

The computational techniques and algorithms are similar to those introduced and described in our previous paper "Shape self-regulation in early lung morphogenesis". In that paper, simulations were computed with Matlab, however in this present work geometrical statistics on large trees were needed and in most cases, the original code was too slow to reach reasonnable computation times. Thus, we implemented the code in the free finite elements software Freefem++ (http://www.freefem.org/ff++) and we interfaced it with the free mesh generation software GMSH (http://geuz.org/gmsh). In this paper, all simulation results were obtained from FreeFem++ simulations except simulations using linear growth responses, already carried out under Matlab.

The linear growth response used in this paper writes as follows:

$$f(\nabla c) = \nabla c \tag{1}$$

The sigmoid growth response writes:

$$f(\nabla c) = \tanh(\nabla c/g_s)\ (1 + \tanh((\nabla c - G_0)/\sigma))/2 \tag{2}$$

The prefactor $\tanh(\nabla c/g_s)$ only insures that $f(0) = 0$. In all simulations with a sigmoid growth response, g_s is set to 0.8, G_0 is set to 2.5 and σ is set to 1.4. A sigmoid is a smooth step function. G_0 and σ respectively represent

the "threshold" and the width of the step. The parameters g and λ may vary, and their values are always specified in the paper. The time step is set to $dt = 0.025$ in arbitrary units (AU). The initial epithelial tube has a radius of 0.2 (AU), while the mesothelium has a radius of 1 (AU).

Measurements from simulations

Measurements required extracting a hierarchic skeleton from the simulated trees. For that purpose, we used Matlab to compute the Voronoi diagram of the shape (Figure 1, left). The set of Voronoi points obtained that are inside the shape constitute the skeleton (Figure 1, right). Bifurcations (branching events) are easily detected: a Voronoi point corresponding to a bifurcation point has three neighbours instead of two. Branches are defined by the sets of points between bifurcations. Starting from the very first branch, we are able to browse the tree branch after branch, ordering them according to bifurcations. Thus, a typical branch has four related branches: a mother (previous generation), a sister (same generation), and two daughters (next generation). The following informations are extracted for each branch:

- Position in the tree (generation and related branches: mother, sister, daughters)
- Length (cumulative distance from the first Voronoi point of the branch point to the last Voronoi point of the branch)
- Diameter (two times the mean distance from Voronoi points to the boundary)
- Asymmetry ratio if the branch has two daughters (ratio between the diameters of the daughter branches).

Measurements from Raabe et al. data

In the paper, we used several times measurements taken from Raabe et al. data. We used only human data from the first male individual (segments labeled as D1, D2, D3, D4, D5, D6, D26, D27, D28, D29, D30) in the description of the measurements. Branches were selected only if proper measurements were possible (see Raabe's comments concerning anomalies preventing measurements). Data together with the description of the measurements can be found on the web at:

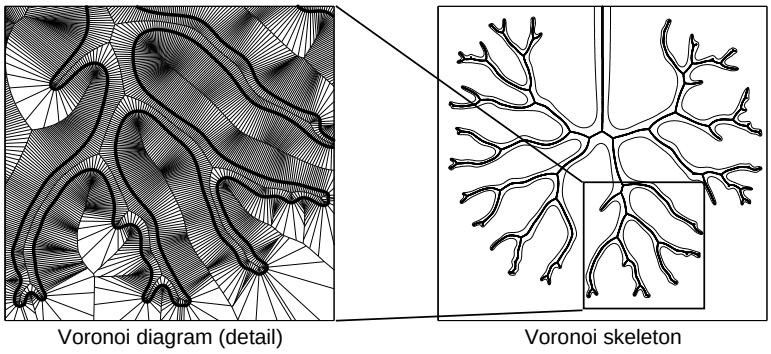

Figure 1: Left: Voronoi diagram of a simulated tree. Only a detail is displayed for readability. Right: skeleton (thick dotted line) obtained from the Voronoi diagram (solid line).

http://mae.ucdavis.edu/wexler/lungs/LF53-Raabe/

3D implementation

The basic algorithm of 3D simulations is similar to the one used in 2D, while the tools are slightly different. FreeFem++ is still used for finite elements solving, Freeyams is used to mesh the epithelial and mesothelial surfaces with triangles of homogeneous sizes, GMSH is used to mesh the mesenchyme volume and Meshfix [1] is used to repair the mesh when required. Figure 2 shows the result of typical simulation. The same striking features are obtained: the initial single tube undergoes repeated branching, with branches diameters distributed around a typical value. Branches are self-avoiding and do not reach the mesothelium (not displayed). Only a few runs were performed in 3D due to important computation times.

Calculations

In this section we provide details concerning the calculations leading to Eq.3 and Eq.4 of the paper. To understand the local dynamics of an epithelial tip (radius of curvature R_e) at distance d from mesothelium (radius of curvature

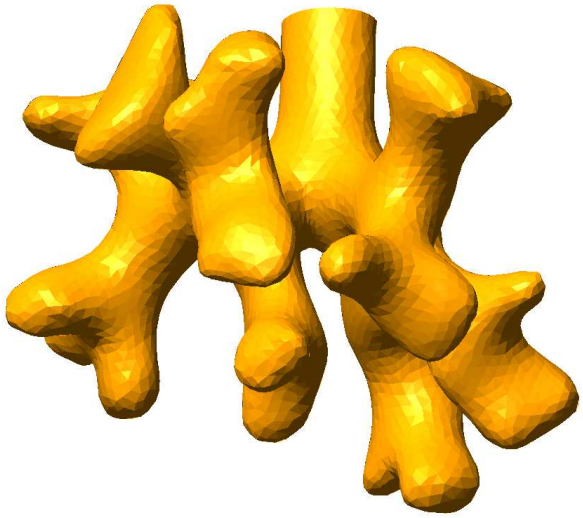

Figure 2: Result of a 3D simulation. Only the epithelium is displayed. Results suggest that the mechanisms are qualitatively similar in 2D and in 3D.

R_m), we first need to calculate the solution of Laplace equation between two non-concentric circles of radii R_e and R_m. The difference of concentration from mesothelium to epithelium is δc, and we define the eccentricity e as $e = R_m - R_e - d$. First, the concentric solution at radius $R_e < r < R_m$ is obtained easily and writes:

$$c(r) = \frac{\delta c}{\ln(R_m/R_e)} \ln(r/R_e) \tag{3}$$

The non-concentric solution can be obtained thanks to a conformal mapping that projects the non-centered circle on a centered one, and leaves the exterior circle unchanged:

$$u(z) = \frac{R_m^2(z-b)}{R_m^2 - bz} \tag{4}$$

The non-concentric solution then reads:

$$c(x,y) = \delta c \left(1 + \alpha \ln\left(R_m^2 \frac{(x-b)^2 + y^2}{(R_m^2 - bx)^2 + (by)^2}\right)\right) \tag{5}$$

with parameter b:

$$b = \frac{1}{2e}\left((R_m^2 - R_e^2 + e^2) \pm \sqrt{(R_m^2 - R_e^2 + e^2)^2 - (2eR_m)^2}\right), \tag{6}$$

and α :

$$\alpha = \left(\ln\left(\frac{b(R_m^2 - eb)}{R_m^2(b-e)}\right)\right)^{-1} \tag{7}$$

We are interested in the gradient of concentration on the epithelium and on the mesothelium. They can be derived easily from the expression of the concentration, and rewritten in terms of the angle θ (with $\theta = 0$ at the tip). For each interface, the angle is defined regarding the center of the corresponding circle. For small values of θ, we have:

$$\begin{cases} (\nabla c)_{epi} = a_e + b_e\ \theta^2 \\ (\nabla c)_{meso} = a_m + b_m\ \theta^2 \end{cases} \tag{8}$$

with

$$a_e = \frac{2\alpha\delta c(R_m^2 - b^2)}{(R_e - b + e)(R_m^2 - bR_e - be)} \tag{9}$$

$$b_e = a_e \frac{R_e(b-e)(R_m^2 - bR_e - be)^2 + bR_e(R_e - b + e)^2(R_m^2 - be)}{2(R_e - b + e)^2(R_m^2 - bR_e - be)^2} \tag{10}$$

$$a_m = \frac{2\alpha\delta c(R_m + b)}{R_m(R_m - b)} \tag{11}$$

$$b_m = a_m \frac{bR_m}{(R_m - b)^2} \tag{12}$$

Like in the simulations, we implement growth as follows:

$$\begin{cases} u_e(\theta) = f((\nabla c)_{epi}) \\ u_m(\theta) = (1+g)\ f((\nabla c)_{meso}) \end{cases} \tag{13}$$

As it depends on the angle θ, growth modifies the radii of curvature R_e and R_m, and consequently the eccentricity e (and distance d). This leads to the final system (used in the section "Epithelium to mesothelium distance" of the paper):

$$\begin{cases} \dot{R}_e = f(a_e) - 2b_e f'(a_e) \\ \dot{R_m} = (1+g)\ [f(a_m) - 2b_m f'(a_m)] \\ \dot{d} = (1+g)\ f(a_m) - f(a_e) \end{cases} \tag{14}$$

References

[1] Marco Attene. A lightweight approach to repairing digitized polygon meshes. *The Visual Computer*, 26:1393–1406, 2010. 10.1007/s00371-010-0416-3.